

A comparison between the one- and two-step spin-orbit coupling approaches based on the *ab initio* Density Matrix Renormalization Group

Huanchen Zhai^{a)} and Garnet Kin-Lic Chan^{b)}

Division of Chemistry and Chemical Engineering, California Institute of Technology, Pasadena, CA 91125, USA

(Dated: 23 September 2022)

The efficient and reliable treatment of both spin-orbit coupling (SOC) and electron correlation is essential for understanding f-element chemistry. We analyze two approaches to the problem, the one-step approach where both effects are treated simultaneously, and the two-step state interaction approach. We report an implementation of the *ab initio* density matrix renormalization group (DMRG) with a one-step treatment of the SOC effect which can be compared to prior two-step treatments on an equal footing. Using a dysprosium octahedral complex and bridged dimer as benchmark systems, we identify characteristics of problems where the one-step approach is beneficial for obtaining the low-energy spectrum.

I. INTRODUCTION

f-element molecules and materials possess unique magnetic and photochemical properties^{1,2} and have been proposed as components of atomic-scale quantum information processing.^{3,4} *Ab initio* electronic structure computation can in principle provide a route to designing the desired f-element chemistry,⁵ however, unlike in lighter element compounds, treating both the strong spin-orbit coupling (SOC) and open-shell electron correlation is essential to establish the qualitative electronic structure.⁶ Commonly, one uses the complete active space self-consistent field (CASSCF) method to treat electron correlation in the f-orbital shell, then treats the SOC interaction in the basis of spin-pure many-electron states. This is the so-called state-interaction spin-orbit (SISO) or 2-step approach.^{7,8}

Although CASSCF-SISO has successfully treated many f-shell (and d-shell) systems,^{9–12} the approach has some limitations. First, in systems with more than a single f-shell atom, the CAS space rapidly becomes too large for exact CASSCF. To address this, approximate correlated electron solvers, such as density matrix renormalization group (DMRG),^{13–30} stochastic heat bath configuration interaction (SHCI),^{31–34} auxiliary-field quantum Monte Carlo (AFQMC)^{35–40}, and full configuration interaction quantum Monte Carlo (FCIQMC)^{41–44} have been explored. Analogous to CASSCF-SISO, such approximate active space solvers can be used in the 2-step state interaction approach, yielding SOC related properties. DMRG-SISO is an example of such a scheme.^{45–48}

Second, there is the potential for the 2-step treatment of SOC to be inefficient when the effects of SOC are large.⁴⁹ Consequently, 1-step approaches to the problem, for example via extensions of CASSCF,⁵⁰ DMRG,⁵¹ SHCI,⁴⁹ and AFQMC⁵² solvers, directly compute eigenstates of the interacting Hamiltonian with SOC. Such

1-step approaches trade the well-optimized and simpler implementation of the spin-free correlation problem with the ability to only compute the eigenstates of interest, and without the need to solve the ancillary state-interaction problem. However, although there are theoretical benefits to the formulation, besides a very recent study based on iterative configuration interaction (iCI),⁵³ we have not found a detailed and quantitative comparison of the performance of the 2-step and 1-step SOC approaches with the same CAS solver, making it difficult to fairly assess the merits of each approach.

In this work, we report a new implementation of *ab initio* DMRG with SOC and electron correlation treated on an equal footing. While our DMRG implementation can handle various relativistic Hamiltonians following an approach similar to the one described in earlier relativistic DMRG studies by Knecht and coworkers,^{54,55} in this work we focus on a treatment via the Spin-Orbit Mean-Field (SOMF) Hamiltonian. We compare the performance of the new 1-step implementation with the existing 2-step DMRG-SISO approach. Based on a theoretical and numerical analysis of the two, we identify a problem where the 1-step SOC approach shows unambiguous advantages. The identified regime should be largely independent of the choice of solver, and thus helps clarify the role of 1-step and 2-step approaches in modeling f-element chemistry.

II. THEORY

A. The Spin-Orbit Mean-Field Hamiltonian

The treatment of relativistic effects in heavy elements can be carried out at different levels of theory⁵⁶. The most direct way is to solve the four-component Dirac-Coulomb-Breit equation. However, this is expensive in complex molecules. Alternatively, one can represent relativistic effects as a correction to non-relativistic quantum chemistry. Namely, we can use a two-component

^{a)}Electronic mail: hczhai@caltech.edu

^{b)}Electronic mail: gkc1000@gmail.com

Hamiltonian of the form^{56,57}

$$\hat{H} = \hat{H}^{\text{SF}} + \hat{H}^{\text{SO}} \quad (1)$$

where \hat{H}^{SF} and \hat{H}^{SO} are the spin-free and spin-orbit coupling terms. Each piece contains relativistic contributions called the scalar relativistic correction and spin-dependent relativistic correction, respectively. As \hat{H}^{SF} has the same form as the non-relativistic Hamiltonian, the structurally new piece is the spin-dependent relativistic correction. The explicit form of the two terms varies with different approximations and implementations. In some special cases, different choices of the relativistic corrections can lead to quantitatively different results.⁴⁹ In this work, we use the Breit-Pauli (BP) version of \hat{H}^{SO} within the SOMF approximation;⁵⁸ alternative types of \hat{H}^{SO} starting from the X2C framework^{59–61} could also be considered. However, we will not discuss the merits of different approximate corrections, but instead only focus on the accuracy and efficiency of the implementation at the correlated electron level.

To formulate the electron correlation problem, we work in an all-electron basis of self-consistent field (SCF) molecular orbitals. For this purpose, we do not use a spin-dependent relativistic correction at the SCF level. The molecular orbitals $\{\phi_i(\mathbf{x})\}$ are then spin-independent real functions. In the molecular orbital basis, the spin-free Hamiltonian resembles its non-relativistic counterpart⁶²

$$\hat{H}^{\text{SF}} := \sum_{ij} t_{ij}^{\text{SF}} \hat{E}_{ij} + \frac{1}{2} \sum_{ijkl} v_{ijkl}^{\text{SF}} \hat{E}_{ijkl} \quad (2)$$

where the singlet excitation operators are given by

$$\begin{aligned} \hat{E}_{ij} &= \sum_{\sigma} a_{i\sigma}^{\dagger} a_{j\sigma} \\ \hat{E}_{ijkl} &= \sum_{\sigma\sigma'} a_{i\sigma}^{\dagger} a_{k\sigma'}^{\dagger} a_{l\sigma'} a_{j\sigma} \end{aligned} \quad (3)$$

and

$$\begin{aligned} t_{ij}^{\text{SF}} &= \int d\mathbf{x} \phi_i^*(\mathbf{x}) \left(-\frac{1}{2} \nabla^2 - \sum_a \frac{Z_a}{r_a} \right) \phi_j(\mathbf{x}) \\ v_{ijkl}^{\text{SF}} &= \int d\mathbf{x}_1 d\mathbf{x}_2 \frac{\phi_i^*(\mathbf{x}_1) \phi_k^*(\mathbf{x}_2) \phi_l(\mathbf{x}_2) \phi_j(\mathbf{x}_1)}{r_{12}} \end{aligned} \quad (4)$$

are the ordinary real-number-valued one- and two-electron integrals, respectively, with the following permutation symmetries

$$\begin{aligned} t_{ij}^{\text{SF}} &= t_{ji}^{\text{SF}} \\ v_{ijkl}^{\text{SF}} &= v_{jikl}^{\text{SF}} = v_{ijlk}^{\text{SF}} = v_{klji}^{\text{SF}} \\ &= v_{jilk}^{\text{SF}} = v_{lkij}^{\text{SF}} = v_{klji}^{\text{SF}} \end{aligned} \quad (5)$$

To appropriately account for the spin-independent relativistic effects for heavy elements, for the applications in this work we compute the molecular orbitals using the

spin-free X2C Hamiltonian, i.e. we use the spin-free X2C one-electron integrals t_{ij}^{SFX2C} in place of t_{ij}^{SF} . Since the total and projected spin are good quantum numbers for the spin-free Hamiltonian

$$[\hat{H}^{\text{SF}}, \hat{S}^2] = [\hat{H}^{\text{SF}}, \hat{S}_z] = 0, \quad (6)$$

the SU(2) symmetry and block-diagonal structure of the Hamiltonian can be utilized to accelerate the computation of the non-relativistic many-body problem. Examples of the usage of these symmetries in DMRG are discussed in Ref. 24 and Ref. 26.

For the BP-SOMF spin-dependent Hamiltonian term, the explicit definitions can be written as

$$\hat{H}^{\text{SO}} := \sum_{ij} \mathbf{t}_{ij}^{\text{SOMF}} \cdot \hat{\mathbf{T}}_{ij} \quad (7)$$

where the triplet excitation operators are

$$\begin{aligned} \hat{T}_{ij,x} &= \frac{1}{2} (a_{i\alpha}^{\dagger} a_{j\beta} + a_{i\beta}^{\dagger} a_{j\alpha}) \\ \hat{T}_{ij,y} &= \frac{1}{2i} (a_{i\alpha}^{\dagger} a_{j\beta} - a_{i\beta}^{\dagger} a_{j\alpha}) \\ \hat{T}_{ij,z} &= \frac{1}{2} (a_{i\alpha}^{\dagger} a_{j\alpha} - a_{i\beta}^{\dagger} a_{j\beta}) \end{aligned} \quad (8)$$

and

$$\mathbf{t}_{ij}^{\text{SOMF}} = \mathbf{t}_{ij}^{\text{SO}} + \sum_{kl} D_{kl} \left(\mathbf{v}_{ijkl}^{\text{SO}} - \frac{3}{2} \mathbf{v}_{ilkj}^{\text{SO}} - \frac{3}{2} \mathbf{v}_{kjil}^{\text{SO}} \right) \quad (9)$$

are the SOMF effective one-electron integrals, with $[D_{ij}]$ the one-particle density matrix and

$$\begin{aligned} \mathbf{t}_{ij}^{\text{SO}} &= \frac{\alpha^2}{2} \int d\mathbf{x} \phi_i^*(\mathbf{x}) \sum_a \frac{Z_a \hat{\mathbf{L}}_a}{r_a^3} \phi_j(\mathbf{x}) \\ \mathbf{v}_{ijkl}^{\text{SO}} &= -\frac{\alpha^2}{2} \int d\mathbf{x}_1 d\mathbf{x}_2 \frac{\phi_i^*(\mathbf{x}_1) \phi_k^*(\mathbf{x}_2) \hat{\mathbf{L}}_{12} \phi_l(\mathbf{x}_2) \phi_j(\mathbf{x}_1)}{r_{12}^3} \end{aligned} \quad (10)$$

the spin-orbit one- and two-electron integrals where α is the fine structure constant and $\hat{\mathbf{L}}$ is the orbital angular momentum operator.

Neither the total spin nor projected spin is conserved in \hat{H}^{SO} . Therefore, the block-diagonal sparse structure (with respect to spin quantum numbers) of the non-relativistic Hamiltonian is lost in \hat{H} . In addition, the $\mathbf{t}_{ij}^{\text{SOMF}}$ matrix elements are complex numbers.

B. The 1- and 2-Step Approaches

In many systems involving third and fourth row transition metals, the effect of the spin-dependent term is relatively small, thus \hat{H}^{SO} can be thought of as a perturbation to the spin-free Hamiltonian. The 2-step or state interaction approach is based on this idea. In the 2-step approach, we first solve the spin-free many-electron eigenvalue problem⁴⁷

$$\hat{H}^{\text{SF}} |\Psi_{S,k}^{\text{SF}}\rangle = E_{S,k}^{\text{SF}} |\Psi_{S,k}^{\text{SF}}\rangle \quad (11)$$

to obtain a small set of spin-pure low-energy eigenstates $|\Psi_{S,k}^{\text{SF}}\rangle$, where the subscript S labels the total spin of the state. Then the relativistic Hamiltonian \hat{H} is constructed and diagonalized in the basis of these spin-pure states. Namely, we consider the effective Hamiltonian with matrix elements

$$\hat{H}_{S_i S_j, i j}^{\text{eff}} = E_{S_i, i}^{\text{SF}} \delta_{i j} \delta_{S_i S_j} + \langle \Psi_{S_i, i}^{\text{SF}} | \hat{H}^{\text{SO}} | \Psi_{S_j, j}^{\text{SF}} \rangle \quad (12)$$

and the SOC corrected energy spectrum is obtained by diagonalizing the small effective Hamiltonian matrix

$$\hat{H}^{\text{eff}} |\Psi_m^{[2]}\rangle = E_m^{[2]} |\Psi_m^{[2]}\rangle \quad (13)$$

where the superscript [2] denotes a quantity obtained from a 2-step treatment.

In contrast, the 1-step approach solves the many-electron eigenvalue problem for \hat{H} directly⁵⁰

$$\hat{H} |\Psi_m^{[1]}\rangle = E_m^{[1]} |\Psi_m^{[1]}\rangle \quad (14)$$

In the weak SOC regime, the 2-step approach has the following characteristics:

(i) Accuracy. The accuracy can be systematically improved by including more low-energy spin-pure states. For some problems, symmetry analysis of the spin-pure states can be utilized to reduce the size of the effective problem.⁴⁷

(ii) Efficiency. Given an existing performant non-relativistic code, the implementation can be optimized with little effort. The most time-consuming parts are obtaining eigenstates of the spin-free Hamiltonian and evaluating the one-particle triplet transition density matrix (1TTDM) between spin-free states. Both computations can reuse highly optimized non-relativistic quantum chemistry subroutines. In addition, the non-relativistic problem has SU(2) symmetry and spatial symmetry with only real-number-valued integrals. Finally, when the spin-free states are labelled by their total spin, the 1TTDM has a band sparse structure, since

$$\langle \Psi_{S_i, i}^{\text{SF}} | \hat{H}^{\text{SO}} | \Psi_{S_j, j}^{\text{SF}} \rangle = 0 \quad (|S_i - S_j| > 1) \quad (15)$$

These features all help to make the computations efficient.

(iii) Dynamic correlation. Non-relativistic dynamic correlation can be approximately included by shifting the diagonal elements of the effective problem.⁵⁰

(iv) Interpretability. The 2-step approach yields the connection between the spin-mixed and spin-pure states as a byproduct. This can be useful for visualization and analysis.

However, we emphasize that the above features of the 2-step approach require the SOC to be small (relative to other electronic effects). When SOC is strong, some of the advantages of the 2-step approach are lost. In such a setting, we have the following considerations:

(i) Accuracy. When \hat{H}^{SO} is large, the eigenstates of \hat{H}^{SF} may poorly approximate the eigenstates of the full

two-component Hamiltonian.⁶ Then, the 2-step approach will converge slowly with respect to the number of spin-pure eigenstates. Some studies have shown that one may need thousands of states per spin multiplicity to obtain reliable results for certain systems.¹² Slow convergence is a particular problem in larger active spaces where the CAS calculation is expensive.

(ii) Numerical conditioning. In an iterative eigenvalue solver such as the Davidson solver, it is relatively easy to find the lowest eigenstates because the energy gaps are relatively large. When targeting the interior eigenvalues however, the gaps are likely to almost vanish. A significantly larger number of iterations must then be used to converge those roots.⁶³ In contrast, the spectrum of the full relativistic Hamiltonian may have much larger gaps when the SOC effect is large, and typically we are only interested in a small number of SOC eigenstates. The numerical conditioning can result in the eigenvalue problem of the full Hamiltonian being easier than the non-relativistic one, and the gain in efficiency from the small number of solver iterations in the 1-step approach may offset the increased cost of removing symmetries present in the 2-step approach.

(iii) Generalisability. The 2-step approach involves two separate eigenvalue problems (the spin-free eigenvalue problem and the state-interaction eigenvalue problem). This complicates the generalization to further computations, such as to obtain response properties. In contrast, the 1-step approach retains the basic theoretical many-body structure of the spin-free many-body computation, with the exception of loss of symmetry. Thus it is easier to derive gradient and response expressions as analogs of those used in the spin-free theory.

Considering the above arguments, we can propose a theoretical regime where the 1-step approach should be computationally superior to the 2-step approach. In particular, the 1-step formalism should possess advantages when (i) SOC is strong, (ii) the number of SOC eigenstates required is small, (iii) the size of the active space is large, and (iv) when we wish to obtain properties in addition to the energy.

C. The DMRG Implementation

To understand the relative performance of the 1-step and 2-step approaches in a system with both strong SOC and electron correlation, we have implemented both approaches using the DMRG algorithm as the CAS solver. As the treatment of dynamic correlation effects (such as through NEVPT2^{64,65}) in the 1- and 2-step calculations is not strictly comparable (see Section IIB), we do not consider dynamic correlation outside the CAS space in this work.

The detailed description of the DMRG-SOSI (2-step) approach can be found in Ref. 47. The main part of a DMRG-SOSI implementation is the spin-adapted *ab initio* DMRG algorithm without the use of singlet embed-

ding^{24,66} (since it is not clear how one can use singlet embedding to compute the 1TTDM between states with different total spins). We re-implemented the DMRG-SOSI approach in the DMRG code BLOCK2⁶⁷ using atomic integrals and SCF solutions computed using PySCF.^{68,69}

The 1-step approach requires extending the DMRG code to support complex number arithmetic. In addition, for the 1-step approach, it is advantageous to work in a general spin orbital formalism. We use a matrix product operator (MPO) in the general spin orbital basis in our implementation. Based on this, all normal/complementary operator indices are spin orbital indices. The DMRG formulae for a general spin orbital implementation can be found in some other publications.^{15,23,70}

The simplest implementation stores all MPO and matrix product state (MPS) data as complex numbers. However, since the two-body part of the MPO and the rotation matrices in the MPS are actually real-number-valued, there will be many exact zeroes in the imaginary part of their representation. Using the floating point number compression method introduced in Ref. 30, these zeroes incur only a negligible amount of disk storage. Nevertheless, the memory and computational costs do not take these zeroes into account. Ideally, one would use the sub-Hamiltonian approach^{23,30} to represent the spin-free part and (pure imaginary part of) the spin-orbit piece of the Hamiltonian as two independent sub-MPOs. Then we could represent the first sub-MPO using only real numbers, reducing memory and computational costs while keeping the accuracy unchanged, since we only require complex-valued computations for the second sub-MPO which does not involve two-electron integrals (when SOMF is used). In practice, however, we found the efficiency of the hybrid scheme to depend greatly on some implementation details. Thus in this work, we report results from the 1-step approach using the single complex MPO, with the MPO automatically constructed using the bipartite matching scheme described in Ref. 70.

III. NUMERICAL EXAMPLE

A. d-element Systems

To benchmark the accuracy of our new SOC-DMRG implementation, we first consider some d-element atoms. We computed the zero-field splitting (ZFS) between the $^2S_{1/2}$ and $^2D_{5/2}$ and $^2D_{3/2}$ states for the Cu and Au atoms,⁴⁷ using the ANO-RCC basis⁷¹ contracted to 6s5p3d2f for Cu and 8s7p4d2f for Au, respectively. We performed the CASSCF calculation with an 11 electron, 11 orbital active space and including 6 doublets in the state-averaged treatment and the 2-step DMRG. We list the results in Table I. The computed splittings agree well with previous theoretical studies and their experimental values.

TABLE I. ZFS for the Cu and Au atoms computed using DMRG-CASSCF (in eV).

term	1-step SOC	2-step SOC	2-step SOC ⁴⁷	experiment ⁷²
Cu atom with CASSCF(11e, 11o) orbitals				
$^2D_{5/2}$	1.568	1.568	1.57	1.39
$^2D_{3/2}$	1.829	1.828	1.83	1.64
$^2D_{5/2} - ^2D_{3/2}$	0.261	0.260	0.26	0.25
Au atom with CASSCF(11e, 11o) orbitals				
$^2D_{5/2}$	1.679	1.652	1.68	1.14
$^2D_{3/2}$	3.416	3.365	3.39	2.66
$^2D_{5/2} - ^2D_{3/2}$	1.737	1.714	1.71	1.52

B. f-element Systems

To further investigate the performance of the 1- and 2-step DMRG-SOC implementations, we consider an artificial f-element molecule, the edge-sharing (bridged) dysprosium dimer complex $[Dy_2Cl_{10}]^{4-}$. Each Dy atom is in an octahedral crystal field, shown in Fig. 1. The corresponding monomer $[DyCl_6]^{3-}$ has been studied in Ref. 73 where the standard CASSCF / NEVPT^{264,65} 2-step approach was used. In this work, we set the $Dy^{III} - Cl^-$ bond length to 2.72 Å according to Table 3 in Ref. 73, which is the optimized bond length found in the octahedral $Dy^{III}Cl_6Na_6$ model.

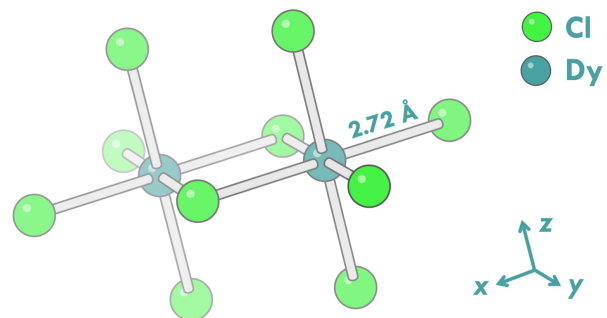


FIG. 1. The geometry of the dysprosium dimer complex $[Dy_2Cl_{10}]^{4-}$.

For the mean-field calculations, we first performed an unrestricted Kohn-Sham (UKS) calculation with the BP86 functional.^{74,75} The Dy and Cl atoms were described by the ANO-RCC basis set⁷¹, contracted to 7s6p4d2f for Dy and 4s3p for Cl, respectively. The mean-field model then has 306 electrons in 248 spatial orbitals in the dimer case. To generate the orbital space for the DMRG calculations, we performed UKS with the high

spin $S_z = 5/2$ (monomer) or $S_z = 5$ (dimer) state. The obtained orbitals were split-localized using the Pipek-Mezey algorithm.⁷⁶ The selected CAS configuration interaction (CASCI) space consisted of 30 electrons in 20 spatial orbitals (i.e. 40 spin orbitals) containing the 14 Dy 4f and 6 bridging Cl p orbitals for the dimer, or 9 electrons in 7 Dy 4f spatial orbitals for the monomer. For the monomer case, we optimized the orbitals using state-averaged CASSCF over 42 doublets, 42 quartets, and 21 sextets, while for the dimer case the orbitals were not optimized.

We determined the ordering of the orbitals used in the 1- and 2-step DMRG using the Fiedler²⁵ scheme. We used the state-averaged DMRG algorithm to obtain the ground and excited states. Note that the state-averaged algorithm over a given number of states N_{av} does not necessarily converge to the lowest N_{av} states (for example, depending on the initial guesses, some excited states might be missed) but will converge to a set of eigenstates at large DMRG bond dimension.

For the dimer case where a large number of states were included in the state-averaged treatment, we further refined the eigenstates using the level-shifted Hamiltonian

$$\hat{H}'_k = \hat{H} + \sum_{i=1}^{k-1} w_i |\Psi_i\rangle\langle\Psi_i| \quad (16)$$

where $|\Psi_i\rangle$ are known (refined) states with energies below the targeted excited state $|\Psi_k\rangle$, and w_i are the weights (energy level shifts). In this work, we set $w_i = 0.5$ Hartree. The additional energy gain from refinement was quite small for the 2-step approach; in the spin-pure case, the improvement from refining the state energies was mostly less than 30 cm^{-1} , with a few cases near 50 cm^{-1} , when averaging over 36 multiplets in each multiplicity. Consequently, to reduce the total wall time for the 2-step approach, the 1TTDM was computed using the state-averaged states, rather than state-specific refined states. For the 1-step approach, we report the energies after this refinement.

The UKS calculations with orbital localization were performed using PySCF^{68,69} with some helper functions from LIBDMET.⁷⁷ The SOMF integrals were obtained from PySCF. All DMRG calculations were performed in BLOCK2.³⁰ The calculations were executed on nodes with 28-core Intel Cascade Lake CPUs (2.2 GHz), made available via the Caltech high-performance computing facility. Each node has 56 CPU cores and 384 GB of memory. For the dimer calculations, each DMRG job used 1 or 2 nodes. For the 2-step approach the main parallelism is over computations of states with different spin multiplicities. We set the MPS bond dimension $M = 2000$ in all DMRG calculations, and the final discarded weight is below 1×10^{-5} for both the 1- and 2-step calculations.

1. Low-Energy Spectra

We plot the low-energy spectra of the dysprosium monomer and dimer complexes studied in this work in Fig. 2 and Fig. 3, respectively. For the no-SOC case, each single level represents an entire spin multiplet. The lowest 11 and 216 multiplets, corresponding to 66 and 1296 eigenstates, are shown for the monomer and dimer respectively. For the 1- and 2-step approaches, the lowest 16 (or 20) spin-mixed eigenstates with SOC corrected energies are shown for the monomer and dimer. As the 1-step approach energies are converged with respect to the DMRG bond dimension, they can be considered to provide reference SOC energies for the eigenstates (although as discussed above, it is not guaranteed that the set of eigenstates are the lowest set). For ease of comparison, the ground-state energies are shifted to a common zero.

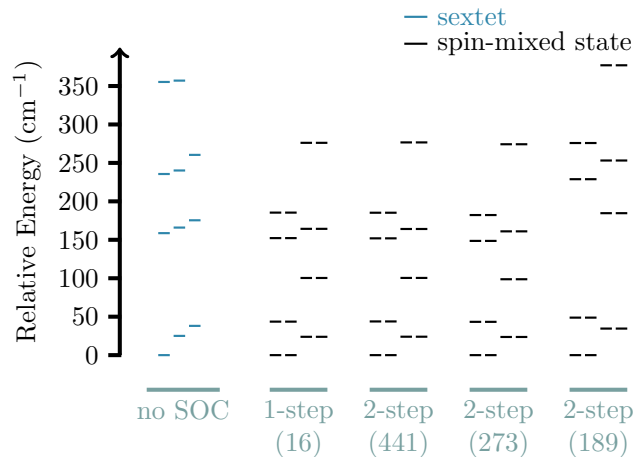


FIG. 2. Low-energy spectrum of $[\text{DyCl}_6]^{3-}$ with CAS(9e, 7o) obtained from DMRG without SOC and 1- and 2-step DMRG-SOC approaches. Spin multiplets and spin-mixed states are shown as colored and black bars, respectively. Arbitrary horizontal shifts are used to separate the near-degenerate states. The numbers in parentheses indicate the total number of states used in the state-averaged DMRG in the 1-step approach or the first step of the 2-step approach.

In the monomer, the large SOC is reflected in the very different number of states at low energy in the no-SOC data versus the SOC spectra. In the case of no-SOC, there are only 6 states below 200 cm^{-1} (all from sextets), while with SOC there are 14 states in this energy window. The ground-state shift due to SOC is -6375 cm^{-1} (not shown in the figure). To obtain qualitative agreement between the 2-step and 1-step spectra for the lowest 16 states, we find that we need to use 42 doublets, 42 quartets, and 21 sextets (273 spin-free states in total) in the 2-step state-interaction problem. When we use 84 doublets, 84 quartets, and 21 sextets (441 spin-free states in total), we find excellent agreement between the 2-step and 1-step spectra. Note that for this CAS(9e, 7o) problem, the full spin-free spectrum contains 490 doublets,

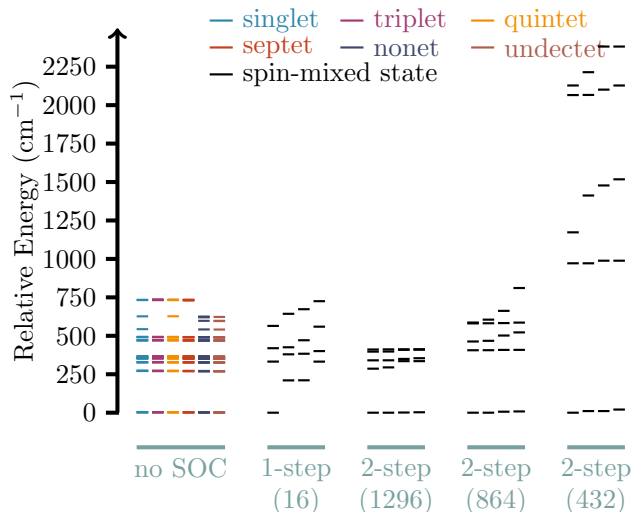


FIG. 3. Low-energy spectrum of $[\text{Dy}_2\text{Cl}_{10}]^{4-}$ with CAS(30e, 20o) obtained from DMRG without SOC and 1- and 2-step DMRG-SOC approaches. Notation is the same as in the previous figure.

224 quartets, and 21 sextets.

In the dimer, the no-SOC spectra for different spin multiplicities are very similar. This indicates that the Heisenberg J coupling between the two metal centers is very weak. Because of this, obtaining a precise value for J requires a more detailed treatment of dynamical correlation and its balance between different states, which is outside the scope of this work. Above 200 cm^{-1} , the density of states is very high (not fully shown in the figure). Each multiplicity has the same number of states in the state-average, and because of the small J coupling, we would expect all the eigenstates to have similar energies. However, we observe that the state-averaged calculations for different multiplicities do not yield all similar energy levels (and thus miss some of the eigenstates). The high density of excited states in the no-SOC spectra not only makes the spin-free calculation harder to converge but also introduces difficulties in selecting spin-free states for the state interaction treatment, since many states can contribute similarly in the SOC treatment.

Similarly to the monomer, the SOC-corrected spectra are quite different from the no-SOC spectra, only more so due to the high density of states in the no-SOC spectrum. In fact, the state-averaged 1-step calculations find only 11 spin-mixed states within the energy range of 500 cm^{-1} above the ground-state, as compared to 1152 spin-free states. The SOC correction for the absolute energy of the ground state is -12723 cm^{-1} (not shown in the figure).

To obtain a similar result to the reference 1-step spectrum using the 2-step approach, we mainly considered 3 different settings, with 12, 24, and 36 multiplets per multiplicity (possible multiplicities were 1,3,5,7,9, and 11) used in the state interaction treatment, respectively. These choices generated in total 432, 864, and 1296 spin-

free states. Fig. 3 illustrates that due to the insufficient number of spin-free states used in the 2-step treatment, the difference between the 1- and 2-step spectra is very large.

2. Convergence

Fig. 4 shows the convergence of the excitation energies and squared total spin $\langle \hat{S}^2 \rangle$ from 2-step to 1-step for the monomer. We see that the convergence with respect to the number of states included in the 2-step approach is faster for the energy than for $\langle \hat{S}^2 \rangle$. From the 1-step calculation, we see that the monomer ground state $\langle \hat{S}^2 \rangle$ is 8.48, which is very close to that of the pure sextet $(\frac{5}{2}(\frac{5}{2} + 1) = 8.75)$. In the dimer case, there is no systematic convergence in the 2-step approach as the number of states is increased. This is seen in Table II, which shows the $\langle \hat{S}^2 \rangle$ values for the lowest 5 states as a function of the number of averaged states in the 2-step approach. Additional information on the energies and $\langle \hat{S}^2 \rangle$ values for the lowest states can be found in the Supporting Information.

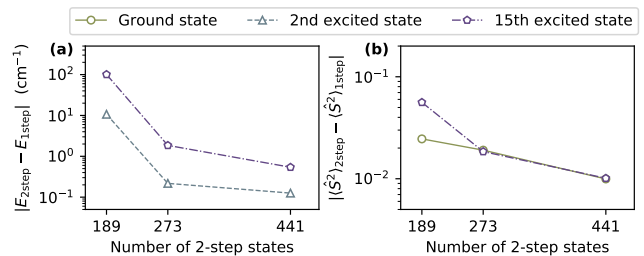


FIG. 4. The difference between representative low-energy states computed from 1-step and 2-step approaches, in (a) excitation energy and (b) $\langle \hat{S}^2 \rangle$ for the monomer.

TABLE II. $\langle \hat{S}^2 \rangle$ computed from 1-step and 2-step approaches for the lowest five states of the dimer. Note that the results from 2-step calculations with more than 1296 spin-pure states may not be fully converged.

SOC scheme	$\langle \hat{S}^2 \rangle$				
1-step (16)	28.9	27.3	26.6	25.1	25.2
2-step (432)	4.98	30.0	30.0	5.01	29.8
2-step (864)	29.9	29.9	5.07	5.06	18.9
2-step (1296)	29.9	29.9	5.09	5.09	7.50
2-step (1728)	29.9	29.9	5.05	5.09	7.74
2-step (2592)	30.0	30.0	29.6	29.6	25.9

3. Efficiency

We list timings for the dimer DMRG calculations performed in this work in Table III. For the 2-step approach, we performed DMRG calculations for each spin multiplicity separately, thus the listed CPU hours are the sums of the CPU hours from all multiplicities. Note that the timings can depend on details of the DMRG parameters and implementation. Also the meaning of the MPS bond dimension M for the general spin MPS and spin-adapted MPS is different, so an absolutely fair comparison is quite difficult. Nevertheless, we see that the 1-step state-averaged DMRG calculations generally incur significant overhead over the 2-step state-averaged calculations. This is mainly because we have to use complex-valued MPS and a general spin MPO for the 1-step Hamiltonian. Nonetheless, when computing 16 states in the 1-step approach, the cost was of the same order of magnitude as that of the spin-free part of the 2-step approach computing hundreds of states. However, the second part of the 2-step approach requires computing the 1TTDM. The computational cost to obtain the 1TTDM increases rapidly with the number of interacting states. Therefore, we find that the total CPU cost required for a reliable 2-step calculation is in fact significantly greater than that required for a 1-step calculation.

TABLE III. Measured and estimated timings for the 1- and 2-step approaches for the dimer.

total CPU hours	1-step (16)	2-step (1296)	2-step (864)	2-step (432)
DMRG	6889	7487	5086	2958
1TTDM	0	2039	907	206

IV. CONCLUSIONS

In this work we carefully analyzed the relative strengths and shortcomings of 1-step and 2-step approaches to treating spin-orbit coupling, using the context of a new DMRG implementation as an example. In numerical tests on a dysprosium dimer complex, we showed that the 1-step approach is preferred when computing the low-energy spectrum due to the strong spin-orbit coupling and high density of states. In particular, the 2-step approach converges very slowly with the number of included spin-free states. For less symmetric systems, the density of states may be lower than the example considered in this work, and this may alleviate some of the problems of the 2-step approach even when the SOC is strong.

In problems of electronic structure with a large amount of degeneracy in the spin-free spectrum, strong SOC can split the degeneracy. In those cases, treating the SOC and non-dynamic correlation simultaneously may be easier since the spin-mixed states will be well separated from

each other. The remaining problem then becomes how to efficiently compute with the more complicated Hamiltonian. As shown in this work in the case of the DMRG implementation, there remains significant overhead when working with two component Hamiltonians. This may be addressed in future work.

ACKNOWLEDGMENTS

This work was supported by the US Department of Energy, Office of Science, via award DE-SC0019390. HZ thanks Zhi-Hao Cui for useful discussions on mean-field calculation and high performance computing strategies, and Xubo Wang for discussions on relativistic Hamiltonians and spin-orbit effective core potentials. The computations presented in this work were conducted at the Resnick High Performance Computing Center, a facility supported by the Resnick Sustainability Institute at the California Institute of Technology.

AUTHOR DECLARATIONS

The authors have no conflicts to disclose.

DATA AVAILABILITY

The data presented in this work can be reproduced using the open-source PYSCF 2.0.1,^{68,69} BLOCK2 0.5.1,⁶⁷ and LIBDMET 0.4⁷⁸ codes. The reference input and output files can be found in the GitHub repo <https://github.com/hczhai/dmrg-soc-data>.

- ¹Lucaccini, E.; Sorace, L.; Perfetti, M.; Costes, J.-P.; Sessoli, R. Beyond the anisotropy barrier: slow relaxation of the magnetization in both easy-axis and easy-plane Ln (trensal) complexes. *Chemical Communications* **2014**, *50*, 1648–1651.
- ²Buenzli, J.-C. G. On the design of highly luminescent lanthanide complexes. *Coordination Chemistry Reviews* **2015**, *293*, 19–47.
- ³Gaita-Ariño, A.; Luis, F.; Hill, S.; Coronado, E. Molecular spins for quantum computation. *Nature chemistry* **2019**, *11*, 301–309.
- ⁴Aguilà, D.; Barrios, L. A.; Velasco, V.; Roubeau, O.; Repollés, A.; Alonso, P. J.; Sesé, J.; Teat, S. J.; Luis, F.; Aromí, G. Heterodimetallic [LnLn'] lanthanide complexes: toward a chemical design of two-qubit molecular spin quantum gates. *Journal of the American Chemical Society* **2014**, *136*, 14215–14222.
- ⁵Böhme, M.; Plass, W. How to link theory and experiment for single-chain magnets beyond the Ising model: magnetic properties modeled from ab initio calculations of molecular fragments. *Chemical science* **2019**, *10*, 9189–9202.
- ⁶Rinehart, J. D.; Long, J. R. Exploiting single-ion anisotropy in the design of f-element single-molecule magnets. *Chemical Science* **2011**, *2*, 2078–2085.
- ⁷Malmqvist, P.-Å.; Roos, B. O. The CASSCF state interaction method. *Chemical physics letters* **1989**, *155*, 189–194.
- ⁸Malmqvist, P. Å.; Roos, B. O.; Schimmelpfennig, B. The restricted active space (RAS) state interaction approach with spin-orbit coupling. *Chemical physics letters* **2002**, *357*, 230–240.
- ⁹Roos, B. O.; Lindh, R.; Malmqvist, P.-Å.; Veryazov, V.; Widmark, P.-O. Main group atoms and dimers studied with a new

- relativistic ANO basis set. *The Journal of Physical Chemistry A* **2004**, *108*, 2851–2858.
- ¹⁰Vancoillie, S.; Malmqvist, P.-Å.; Pierloot, K. Calculation of EPR g Tensors for Transition-Metal Complexes Based on Multiconfigurational Perturbation Theory (CASPT2). *ChemPhysChem* **2007**, *8*, 1803–1815.
- ¹¹Yadav, R.; Bogdanov, N. A.; Katukuri, V. M.; Nishimoto, S.; Van Den Brink, J.; Hozoi, L. Kitaev exchange and field-induced quantum spin-liquid states in honeycomb α -RuCl₃. *Scientific reports* **2016**, *6*, 1–16.
- ¹²Ungur, L.; Chibotaru, L. F. Ab initio crystal field for lanthanides. *Chem.-Eur. J* **2017**, *23*, 3708–3718.
- ¹³White, S. R. Density matrix formulation for quantum renormalization groups. *Physical review letters* **1992**, *69*, 2863.
- ¹⁴White, S. R. Density-matrix algorithms for quantum renormalization groups. *Physical Review B* **1993**, *48*, 10345.
- ¹⁵Chan, G. K.-L.; Head-Gordon, M. Highly correlated calculations with a polynomial cost algorithm: A study of the density matrix renormalization group. *The Journal of chemical physics* **2002**, *116*, 4462–4476.
- ¹⁶Chan, G. K.-L. An algorithm for large scale density matrix renormalization group calculations. *The Journal of chemical physics* **2004**, *120*, 3172–3178.
- ¹⁷Chan, G. K.-L.; Sharma, S. The density matrix renormalization group in quantum chemistry. *Annual review of physical chemistry* **2011**, *62*, 465–481.
- ¹⁸Legeza, Ö.; Röder, J.; Hess, B. Controlling the accuracy of the density-matrix renormalization-group method: The dynamical block state selection approach. *Physical Review B* **2003**, *67*, 125114.
- ¹⁹Barcza, G.; Legeza, Ö.; Marti, K. H.; Reiher, M. Quantum-information analysis of electronic states of different molecular structures. *Physical Review A* **2011**, *83*, 012508.
- ²⁰Baiardi, A.; Reiher, M. The density matrix renormalization group in chemistry and molecular physics: Recent developments and new challenges. *The Journal of Chemical Physics* **2020**, *152*, 040903.
- ²¹Brabec, J.; Brandejs, J.; Kowalski, K.; Xantheas, S.; Legeza, Ö.; Veis, L. Massively parallel quantum chemical density matrix renormalization group method. *Journal of Computational Chemistry* **2021**, *42*, 534–544.
- ²²Mitrushenkov, A. O.; Fano, G.; Ortolani, F.; Linguerrì, R.; Palmieri, P. Quantum chemistry using the density matrix renormalization group. *The Journal of Chemical Physics* **2001**, *115*, 6815–6821.
- ²³Chan, G. K.-L.; Keselman, A.; Nakatani, N.; Li, Z.; White, S. R. Matrix product operators, matrix product states, and ab initio density matrix renormalization group algorithms. *The Journal of chemical physics* **2016**, *145*, 014102.
- ²⁴Sharma, S.; Chan, G. K.-L. Spin-adapted density matrix renormalization group algorithms for quantum chemistry. *The Journal of chemical physics* **2012**, *136*, 124121.
- ²⁵Olivares-Amaya, R.; Hu, W.; Nakatani, N.; Sharma, S.; Yang, J.; Chan, G. K.-L. The ab-initio density matrix renormalization group in practice. *The Journal of chemical physics* **2015**, *142*, 034102.
- ²⁶Wouters, S.; Poelmans, W.; Ayers, P. W.; Van Neck, D. CheMPS2: A free open-source spin-adapted implementation of the density matrix renormalization group for ab initio quantum chemistry. *Computer Physics Communications* **2014**, *185*, 1501–1514.
- ²⁷Wouters, S.; Van Neck, D. The density matrix renormalization group for ab initio quantum chemistry. *The European Physical Journal D* **2014**, *68*, 272.
- ²⁸Keller, S.; Dolfi, M.; Troyer, M.; Reiher, M. An efficient matrix product operator representation of the quantum chemical Hamiltonian. *The Journal of chemical physics* **2015**, *143*, 244118.
- ²⁹Keller, S.; Reiher, M. Spin-adapted matrix product states and operators. *The Journal of chemical physics* **2016**, *144*, 134101.
- ³⁰Zhai, H.; Chan, G. K.-L. Low communication high performance ab initio density matrix renormalization group algorithms. *The Journal of Chemical Physics* **2021**, *154*, 224116.
- ³¹Holmes, A. A.; Tubman, N. M.; Umrigar, C. Heat-bath configuration interaction: An efficient selected configuration interaction algorithm inspired by heat-bath sampling. *Journal of chemical theory and computation* **2016**, *12*, 3674–3680.
- ³²Sharma, S.; Holmes, A. A.; Jeanmairet, G.; Alavi, A.; Umrigar, C. J. Semistochastic heat-bath configuration interaction method: Selected configuration interaction with semistochastic perturbation theory. *Journal of chemical theory and computation* **2017**, *13*, 1595–1604.
- ³³Holmes, A. A.; Umrigar, C.; Sharma, S. Excited states using semistochastic heat-bath configuration interaction. *The Journal of chemical physics* **2017**, *147*, 164111.
- ³⁴Smith, J. E.; Mussard, B.; Holmes, A. A.; Sharma, S. Cheap and near exact CASSCF with large active spaces. *Journal of chemical theory and computation* **2017**, *13*, 5468–5478.
- ³⁵Zhang, S.; Krakauer, H. Quantum Monte Carlo method using phase-free random walks with Slater determinants. *Physical review letters* **2003**, *90*, 136401.
- ³⁶Al-Saidi, W.; Zhang, S.; Krakauer, H. Auxiliary-field quantum Monte Carlo calculations of molecular systems with a Gaussian basis. *The Journal of chemical physics* **2006**, *124*, 224101.
- ³⁷Suewattana, M.; Purwanto, W.; Zhang, S.; Krakauer, H.; Walter, E. J. Phaseless auxiliary-field quantum Monte Carlo calculations with plane waves and pseudopotentials: Applications to atoms and molecules. *Physical Review B* **2007**, *75*, 245123.
- ³⁸Purwanto, W.; Al-Saidi, W.; Krakauer, H.; Zhang, S. Eliminating spin contamination in auxiliary-field quantum Monte Carlo: Realistic potential energy curve of F₂. *The Journal of chemical physics* **2008**, *128*, 114309.
- ³⁹Purwanto, W.; Zhang, S.; Krakauer, H. Excited state calculations using phaseless auxiliary-field quantum Monte Carlo: Potential energy curves of low-lying C₂ singlet states. *The Journal of chemical physics* **2009**, *130*, 094107.
- ⁴⁰Motta, M.; Zhang, S. Ab initio computations of molecular systems by the auxiliary-field quantum Monte Carlo method. *Wiley Interdisciplinary Reviews: Computational Molecular Science* **2018**, *8*, e1364.
- ⁴¹Booth, G. H.; Thom, A. J.; Alavi, A. Fermion Monte Carlo without fixed nodes: A game of life, death, and annihilation in Slater determinant space. *The Journal of chemical physics* **2009**, *131*, 054106.
- ⁴²Cleland, D.; Booth, G. H.; Alavi, A. Communications: Survival of the fittest: Accelerating convergence in full configuration-interaction quantum Monte Carlo. *The Journal of chemical physics* **2010**, *132*, 041103.
- ⁴³Booth, G. H.; Grüneis, A.; Kresse, G.; Alavi, A. Towards an exact description of electronic wavefunctions in real solids. *Nature* **2013**, *493*, 365–370.
- ⁴⁴Blunt, N.; Booth, G. H.; Alavi, A. Density matrices in full configuration interaction quantum Monte Carlo: Excited states, transition dipole moments, and parallel distribution. *The Journal of Chemical Physics* **2017**, *146*, 244105.
- ⁴⁵Roemelt, M. Spin orbit coupling for molecular ab initio density matrix renormalization group calculations: Application to g-tensors. *The Journal of chemical physics* **2015**, *143*, 044112.
- ⁴⁶Knecht, S.; Keller, S.; Autschbach, J.; Reiher, M. A nonorthogonal state-interaction approach for matrix product state wave functions. *Journal of chemical theory and computation* **2016**, *12*, 5881–5894.
- ⁴⁷Sayfutyarova, E. R.; Chan, G. K.-L. A state interaction spin-orbit coupling density matrix renormalization group method. *The Journal of chemical physics* **2016**, *144*, 234301.
- ⁴⁸Sayfutyarova, E. R.; Chan, G. K.-L. Electron paramagnetic resonance g-tensors from state interaction spin-orbit coupling density matrix renormalization group. *The Journal of chemical physics* **2018**, *148*, 184103.

- ⁴⁹Mussard, B.; Sharma, S. One-step treatment of spin-orbit coupling and electron correlation in large active spaces. *Journal of chemical theory and computation* **2018**, *14*, 154–165.
- ⁵⁰Ganyushin, D.; Neese, F. A fully variational spin-orbit coupled complete active space self-consistent field approach: Application to electron paramagnetic resonance g-tensors. *The Journal of chemical physics* **2013**, *138*, 104113.
- ⁵¹Hoyer, C. E.; Hu, H.; Lu, L.; Knecht, S.; Li, X. Relativistic Kramers-Unrestricted Exact-Two-Component Density Matrix Renormalization Group. *The Journal of Physical Chemistry A* **2022**.
- ⁵²Eskridge, B.; Krakauer, H.; Shi, H.; Zhang, S. Ab initio calculations in atoms, molecules, and solids, treating spin-orbit coupling and electron interaction on an equal footing. *The Journal of Chemical Physics* **2022**, *156*, 014107.
- ⁵³Zhang, N.; Xiao, Y.; Liu, W. SOiCI and iCISO: combining iterative configuration interaction with spin-orbit coupling in two ways. *Journal of Physics: Condensed Matter* **2022**, *34*, 224007.
- ⁵⁴Knecht, S.; Legeza, Ö.; Reiher, M. Communication: Four-component density matrix renormalization group. *The Journal of chemical physics* **2014**, *140*, 041101.
- ⁵⁵Battaglia, S.; Keller, S.; Knecht, S. Efficient relativistic density-matrix renormalization group implementation in a matrix-product formulation. *Journal of chemical theory and computation* **2018**, *14*, 2353–2369.
- ⁵⁶Dyall, K. G.; Fægri Jr, K. *Introduction to relativistic quantum chemistry*; Oxford University Press, 2007.
- ⁵⁷Reiher, M.; Wolf, A. *Relativistic quantum chemistry: the fundamental theory of molecular science*; John Wiley & Sons, 2014.
- ⁵⁸Neese, F. Efficient and accurate approximations to the molecular spin-orbit coupling operator and their use in molecular g-tensor calculations. *The Journal of chemical physics* **2005**, *122*, 034107.
- ⁵⁹Li, Z.; Xiao, Y.; Liu, W. On the spin separation of algebraic two-component relativistic Hamiltonians: Molecular properties. *The Journal of Chemical Physics* **2014**, *141*, 054111.
- ⁶⁰Liu, J.; Cheng, L. An atomic mean-field spin-orbit approach within exact two-component theory for a non-perturbative treatment of spin-orbit coupling. *The Journal of Chemical Physics* **2018**, *148*, 144108.
- ⁶¹Zhang, C.; Cheng, L. Atomic Mean-Field Approach within Exact Two-Component Theory Based on the Dirac-Coulomb-Breit Hamiltonian. *The Journal of Physical Chemistry A* **2022**, *126*, 4537–4553.
- ⁶²Helgaker, T.; Jorgensen, P.; Olsen, J. *Molecular electronic-structure theory*; John Wiley & Sons, 2014.
- ⁶³Dorando, J. J.; Hachmann, J.; Chan, G. K.-L. Targeted excited state algorithms. *The Journal of chemical physics* **2007**, *127*, 084109.
- ⁶⁴Angeli, C.; Cimraglia, R.; Evangelisti, S.; Leininger, T.; Malrieu, J.-P. Introduction of n-electron valence states for multireference perturbation theory. *The Journal of Chemical Physics* **2001**, *114*, 10252–10264.
- ⁶⁵Angeli, C.; Cimraglia, R.; Malrieu, J.-P. n-electron valence state perturbation theory: A spinless formulation and an efficient implementation of the strongly contracted and of the partially contracted variants. *The Journal of chemical physics* **2002**, *117*, 9138–9153.
- ⁶⁶Li, Z.; Chan, G. K.-L. Spin-projected matrix product states: Versatile tool for strongly correlated systems. *Journal of chemical theory and computation* **2017**, *13*, 2681–2695.
- ⁶⁷Zhai, H.; Larsson, H. R.; Cui, Z.-H.; Lee, S. block2: Efficient MPO implementation of quantum chemistry DMRG. 2021; <https://github.com/block-hczhai/block2-preview>.
- ⁶⁸Sun, Q.; Berkelbach, T. C.; Blunt, N. S.; Booth, G. H.; Guo, S.; Li, Z.; Liu, J.; McClain, J. D.; Sayfutyarova, E. R.; Sharma, S., et al. PySCF: the Python-based simulations of chemistry framework. *Wiley Interdisciplinary Reviews: Computational Molecular Science* **2018**, *8*, e1340.
- ⁶⁹Sun, Q.; Zhang, X.; Banerjee, S.; Bao, P.; Barbry, M.; Blunt, N. S.; Bogdanov, N. A.; Booth, G. H.; Chen, J.; Cui, Z.-H., et al. Recent developments in the PySCF program package. *The Journal of chemical physics* **2020**, *153*, 024109.
- ⁷⁰Ren, J.; Li, W.; Jiang, T.; Shuai, Z. A general automatic method for optimal construction of matrix product operators using bipartite graph theory. *The Journal of Chemical Physics* **2020**, *153*, 084118.
- ⁷¹Roos, B. O.; Lindh, R.; Malmqvist, P.-Å.; Veryazov, V.; Widmark, P.-O. New relativistic ANO basis sets for transition metal atoms. *The Journal of Physical Chemistry A* **2005**, *109*, 6575–6579.
- ⁷²Sansonetti, J. E.; Martin, W. C. Handbook of basic atomic spectroscopic data. *Journal of physical and chemical reference data* **2005**, *34*, 1559–2259.
- ⁷³Aravena, D.; Atanasov, M.; Neese, F. Periodic trends in lanthanide compounds through the eyes of multireference ab initio theory. *Inorganic chemistry* **2016**, *55*, 4457–4469.
- ⁷⁴Perdew, J. P. Density-functional approximation for the correlation energy of the inhomogeneous electron gas. *Physical Review B* **1986**, *33*, 8822.
- ⁷⁵Becke, A. D. Density-functional exchange-energy approximation with correct asymptotic behavior. *Physical review A* **1988**, *38*, 3098.
- ⁷⁶Pipek, J.; Mezey, P. G. A fast intrinsic localization procedure applicable for abinitio and semiempirical linear combination of atomic orbital wave functions. *The Journal of Chemical Physics* **1989**, *90*, 4916–4926.
- ⁷⁷Cui, Z.-H.; Zhai, H.; Zhang, X.; Chan, G. K.-L. Systematic electronic structure in the cuprate parent state from quantum many-body simulations. *Science* **2022**, *377*, 1192–1198.
- ⁷⁸libDMET: A library of density matrix embedding theory (DMET) for lattice models and realistic solids, https://github.com/gkclab/libdmet_preview.